4.6 A-PRIORI LABORATORY STUDY OF SUBFILTER-SCALE MODELS FOR LES OVER HETEROGENEOUS LAND SURFACES

Matthew A. Carper*, Fernando Porté-Agel and Leonardo Chamorro
Saint Anthony Falls Laboratory, Department of Civil Engineering
University of Minnesota, Minneapolis, Minnesota

1. INTRODUCTION

Turbulent fluxes of momentum, heat and moisture within the surface layer of the ABL are well known to be affected by surface heterogeneity (Kaimal and Finnigan, 1994). Large-eddy simulation (LES) provides invaluable insight on the effects of surface heterogeneity on regional-scale turbulent fluxes, which is guiding the development of improved parameterizations of those fluxes in large-scale weather and climate models (e.g., Bou-Zeid *et al.*, 2004; Stoll and Porté-Agel, *JP4.2*). However, recent studies have shown that inhomogeneity and anisotropy of the flow at the smallest resolved and sub-filter scales hinder the performance of subfilter-scale (SFS) models used in LES of boundary layer flows over complex terrain (e.g., Bou-Zeid *et al.*, 2005; Stoll and Porté-Agel, 2006).

In order to test and improve the performance of SFS models and, in turn, of LES, a better understanding of the behavior of the SFS stresses and energy transfers (between resolved and subfilter scales) is required. The SFS stress tensor that needs to be modeled in LES is defined as

$$\tau_{ij} = \widetilde{u_i u_j} - \tilde{u}_i \tilde{u}_j, \tag{1}$$

where the tilde (˜) denotes spatial filtering. The most common model for this stress tensor, an eddy-viscosity model, relates the SFS stress to the resolved strain rate

$$\tau_{ij}^{ev} = -2(C_s \Delta)^2 |\tilde{S}| \tilde{S}_{ij}, \tag{2}$$

where C_s is the so-called Smagorinsky coefficient, Δ is the filter width scale and $\tilde{S}_{ij} = \frac{1}{2}(\frac{\partial \tilde{u_i}}{\partial x_j} + \frac{\partial \tilde{u_j}}{\partial x_i})$ is the filtered strain rate tensor. Simulation results are known to be very sensitive to the way C_s is specified as a function of local flow conditions. Particularly interesting is the recent development and implementation of the so-called dynamic procedures used to optimize the value of C_s as a function of the resolved scales, thus not requiring any *ad hoc* tuning (e.g., Porté-Agel *et al.*, 2000; Bou-Zeid *et al.*, 2005; Stoll and Porté-Agel, 2006).

The effect of the subfilter scales on the resolved turbulent kinetic energy can be quantified through the SFS transfer rate of kinetic energy between resolved and subfilter scales,

$$\Pi = -\tau_{ij} \tilde{S}_{ij}. \tag{3}$$

*Corresponding author address: M.A. Carper, Saint Anthony Falls, Dept. of Civil Engineering, 2 3rd Avenue SE, Minneapolis, MN 55414, e-mail: carper@msi.umn.edu

The ability of SFS models to reproduce mean value of the SFS transfer rate of kinetic energy has been shown to be necessary for a LES to produce accurate flow statistics (Meneveau and Katz, 2000).

In recent years, many *a priori* experimental field and laboratory studies have been designed to study the SFS stresses and transfer rates of kinetic energy (e.g., Liu *et al.*, 1994; Tong *et al.*, 1998; Meneveau and Katz, 2000; Porté-Agel *et al.*, 2001; Kleissl *et al.*, 2004; Sullivan *et al.*, 2003; Higgins *et al.*, 2003; Horst *et al.*, 2004; Carper and Porté-Agel, 2004). These studies have provided important insight to the statistical and geometric properties of those quantities in boundary layers over homogeneous surfaces.

In this study, we present results from a unique wind-tunnel experiment designed to study the effects of surface heterogeneity on SFS stresses and transfer rates of kinetic energy. A boundary layer wind tunnel provides full and accurate control of both surface roughness and flow conditions. In addition, the ability to perform particle image velocimetry (PIV) in the wind tunnel provides high-resolution spatial distribution of the velocity field throughout the boundary layer. These spatially resolved fields are required to apply the spatial filtering operation involved in the calculation of the SFS stresses (Eq. 1) and SFS transfer rate of kinetic energy (Eq. 3). The following section provides an overview of the experiment and preliminary results on the effects of surface-roughness transitions on SFS quantities and SFS model performance.

2. METHODOLOGY

2.1 *Experimental Setup*

In order to properly study the effect of heterogeneous land surfaces on SFS physics, a well defined rough-to-smooth surface transition has been designed and setup in the boundary layer wind tunnel at the Saint Anthony Falls Laboratory at the University of Minnesota (see Fig. 1). This rough-to-smooth transition is created by placing 7 m of wire mesh ($k = 3.0$ mm and $z_{01} = 0.4$ mm) on the wind tunnel floor upstream of an aerodynamically smooth clear-glass plate. This setup allows for particle image velocimetry (PIV) to be performed in the surface layer above the glass plate and for detailed measurements using hot-wire anemometry at various positions downstream of the transition. In this study, a turbulent boundary layer is developed upstream with the help of a tripping mechanism (8 cm picket fence) and is allowed to grow in zero pressure gradient conditions by adjustment of the wind tunnel ceiling. The boundary layer under a 10 m/s free stream

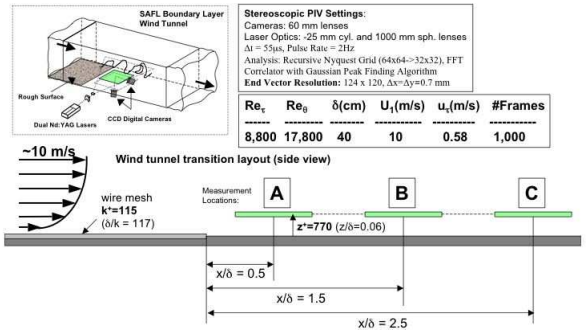

FIG. 1: Diagram of experimental setup in the Saint Anthony Falls boundary layer wind tunnel to study a turbulent boundary layer over a rough-to-smooth transition using stereoscopic particle image velocimetry (PIV) over horizontal planes at three downstream locations.

velocity grows to a height of 40 cm at the transition location. The upstream roughness was chosen to have a height and roughness length that provides a dramatic change in momentum flux near the surface which can be measured with accuracy, while still maintaining a well-developed surface layer with constant shear stress and a logarithmic velocity profile. Past wind tunnel studies over roughness transitions (Antonia and Luxton, 1971, 1972; Mulhearn, 1978; Cheng and Castro, 2002) have provided valuable results and insight but may be regarded as non-typical of land-surface transitions because the effect of their roughness elements reach far into the inner region of the boundary layer and may not provide a large enough range of length scales. Furthermore, a review of research on rough wall boundary layers by Jiménez (2004) has shown that there seems to be a distinct difference between turbulent boundary layers with varying ratios of boundary-layer height to roughness-element height (δ/k) with, seemingly, a change in behavior for boundary layers $\delta/k > 80$ (which is typical for the ABL). The setup we present here maintains a $\delta/k \sim$117 whilst previous studies have $\delta/k \sim$20 (Luxton and Antonia, 1972; Mulhearn, 1978; Cheng and Castro, 2002).

2.2 *Measurements*

Measurements of mean velocity profiles were made using a Pitot-static tube and were calculated based on 60 s time series at each height. The PIV measurements were performed using a TSI stereoscopic *UltraPIV* system. The PIV images are processed using 32x32 pixel interrogation windows in a recursive Nyquist analysis with a FFT correlating engine and a Gaussian peak finding algorithm. For these settings with approximately 10 particle pairs per interrogation window, the expected uncertainty in finding the peak displacement are expected to be 0.1 pixel (Westerweel, 1997). With an average particle image displacement of 8-10 pixels this corresponds to a velocity uncertainty error less than 2%. Images acquired were slightly defocused to increase particle image sizes and, thus, avoid excessive pixel locking errors. Stereoscopic measurements (all three components of velocity) were obtained over the horizontal planes while only the streamwise and vertical components of velocity were obtained over the vertical planes. This was primarily due to illumination constraints of the PIV setup for the vertical planes.

The PIV data consist of both horizontal ($z/\delta = 0.05$, $z^+ = 770$) velocity fields and vertical velocity fields at three different locations downstream of the rough-to-smooth transition: x/δ=0.5 (A), 1.5 (B) and 2.5 (C). The setup for the horizontal stereoscopic PIV measurements is shown in Fig. 1. Horizontal velocity fields span an area of approximately 8 cm$\times$8 cm with a vector spacing of 0.7 mm, whereas vertical velocity fields span an area of approximately 14 cm$\times$14 cm with a spacing of 1.2 mm. In order to have enough data to converge the flow statistics of interest, 1,000 PIV images were acquired for each horizontal position and 3,000 PIV images were acquired for each vertical position. Each velocity field calculated from these images corresponds to roughly 15,000 vectors. Sample velocity fields are shown in Fig. 2 for a vertical field and in Fig. 3 for a horizontal field.

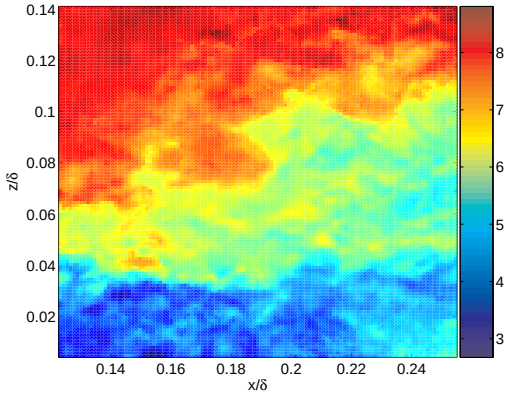

FIG. 2: Streamwise velocity field ($u_1, m/s$) from PIV measurements at x/δ = 0.5 behind a rough-to-smooth surface transition.

2.3 *Flow Characterization*

The zero pressure gradient boundary layer, developed upstream of the transition, has a Reynolds number based on momentum thickness $Re_\theta = 1.8 \times 10^4$, a Reynolds number based on shear stress $Re_\tau = 8.8 \times 10^3$, with a boundary layer height $\delta \approx 40$ cm, friction velocity $u_* = 0.6$ m/s, and a free stream velocity $U_1 = 10$ m/s. The rough surface was a "k-type" roughness (Jiménez, 2004) and consisted of woven-wire mesh with diameter of 1.5 mm, nominal height $k = 3.0$ mm, where $k^+ = 115$ and $\delta/k = 130$. For these conditions, the boundary layer upstream is in the fully rough regime (Jiménez, 2004). The smooth surface is a window of glass that lies flush

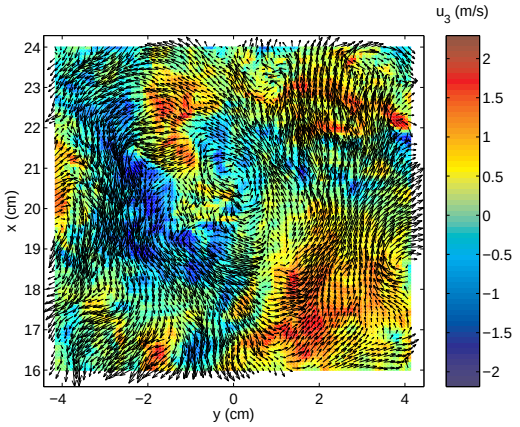

FIG. 3: Horizontal field of vertical velocity overlaid with velocity fluctuation vectors from stereoscopic PIV measurements at x/δ = 0.5 behind a rough-to-smooth surface transition.

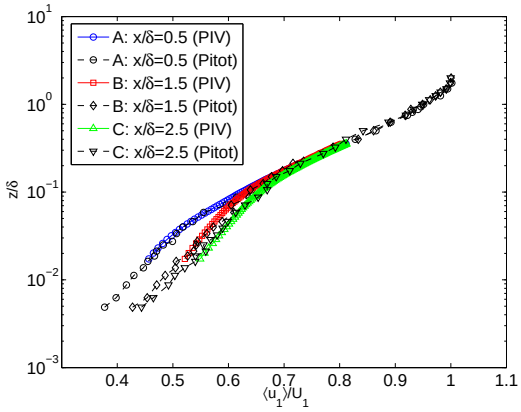

FIG. 4: Mean profiles of the streamwise velocity at three positions downstream of the rough-to-smooth transition.

and sealed with the finished wooden floor of the tunnel. This smooth surface is considered and verified by experiment to be aerodynamically smooth. A roughness length for this smooth surface can be estimated using Clauser's fit of an inertial sublayer (with $\kappa = 0.41$ and $A = 5.0$) to find $z_{02} \sim 0.13\nu/u_*$, which for this case is 0.0036 mm. Using this value, we calculate the strength of the roughness change, M = $ln(z_{01}/z_{02})$, to be $+4.7$. This compares well with Bradley's (1968) field study that had a roughness change of M = ± 4.8.

The effect of the roughness transition is easily seen in the profiles of the mean velocity, as measured with a Pitot-static tube, shown in Fig. 4. The growth of the internal boundary layer (IBL), defined here as the height at which the downstream velocity profile matches within 5% the upstream-rough velocity profile, was shown to follow closely the empirical result of Elliot (1958) modified by Wood (1982) of $z_{IBL}/z_{01} = 0.28(x/z_{01})^{0.8}$. The best fit to the current data was $z_{IBL}/z_{01} = 0.2(x/z_{01})^{0.84}$. The growth rate of the effect of the roughness change on the turbulence in the boundary layer has been shown by previous studies (e.g., Antonia and Luxton, 1972) to be greater than the mean profile. This can be observed by comparing the profiles of the normal and shear turbulent stresses calculated from the unfiltered PIV data and shown in Figs. 5 and 6, respectively.

2.4 *A-priori Evaluation of SFS Quantities*

In order to evaluate the SFS quantities, the experimental data from the PIV measurements must be spatially filtered. To do this, a 2-D spatial box (or tophat) filter is used, defined as

$$G(\mathbf{x}) = \begin{cases} \frac{1}{|G|} & \text{if } \mathbf{x} \le \Delta \\ 0 & \text{if } \mathbf{x} > \Delta \end{cases}$$

$$\hat{G}(\kappa) = \frac{\sin(\frac{1}{2}\kappa\Delta)}{\frac{1}{2}\kappa\Delta}.$$

The filtering process is carried out in two dimensions. For the horizontal fields, the filter used is symmetric and has typical filter widths of $\Delta = \sqrt{\Delta_x \Delta_y} = 0.7$ cm, 1.4 cm and 2.8 cm. These filter widths have been shown to range from falling within the inertial subrange of the kinetic energy spectra to reaching up into production scales (i.e., for $z/\Delta \lesssim 1$). For the vertical fields, the filter is elongated in the streamwise direction with a typical aspect ratio of 6:1 and typical filter widths of $\Delta = \sqrt{\Delta_x \Delta_z} = 1.7$ cm. For the horizontal fields, the filter is square (1:1) and has typical filter widths of $\Delta = 1.0$ cm. A demonstration of this filtering procedure for a vertical field using the vector field shown in Fig. 2 is shown in Fig. 7. Likewise, a filtered horizontal field is shown in Fig. 8, using the vector field shown in Fig. 3. Gradients of filtered quantities are calculated using centered finite differencing across a distance equal to the filter scale, so as to be consistent with gradients available in LES.

Using these filtered velocities and gradients of filtered velocities, the SFS stresses and filtered strain rate tensors (defined in Section 1) are calculated. In order to calculate the SFS transfer rate of kinetic energy (Eq. 3) from the vertical measurements, assumptions are needed to account for the missing spanwise velocity component and spanwise velocity gradients. Similarly, assumptions are needed to use the horizontal PIV data to account for the missing vertical velocity gradients. Therefore, we use surrogates of the SFS transfer rate of kinetic energy based on continuity of the flow and assumptions of local isotropy (similar to Liu *et al.*, 1994), defined for the horizontal fields as

$$\Pi_\Delta^H = -\tfrac{1}{2}(\tau_{11}\tilde{S}_{11} + 4\tau_{12}\tilde{S}_{12} + \tau_{22}\tilde{S}_{22} - \tau_{11}\tilde{S}_{22} - \tau_{22}\tilde{S}_{11} + 2\tau_{13}\tfrac{\partial \tilde{u}_3}{\partial x_1} + 2\tau_{23}\tfrac{\partial \tilde{u}_3}{\partial x_2}), \quad (4)$$

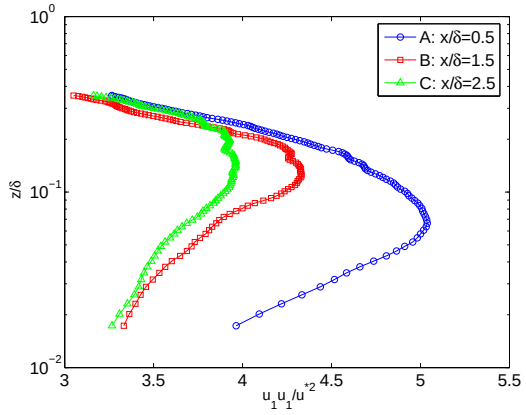

FIG. 5: Mean profiles of the Reynolds' streamwise normal stress at three positions downstream of the rough-to-smooth transition.

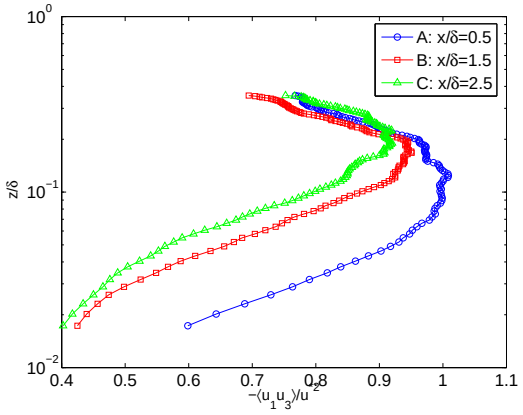

FIG. 6: Mean profiles of the Reynolds' shear stress at three positions downstream of the rough-to-smooth transition.

and for the vertical fields as

$$\Pi^V_\Delta = -\tfrac{1}{2}(\tau_{11}\tilde{S}_{11} + 12\tau_{13}\tilde{S}_{13} - \tau_{11}\tilde{S}_{33} - \tau_{33}\tilde{S}_{11} + \tau_{33}\tilde{S}_{33}). \quad (5)$$

Using these values, the model coefficient C_s^2 can be evaluated directly

$$C_s^2 = \frac{-\langle \tau_{ij}\tilde{S}_{ij}\rangle}{\langle 2\Delta^2|\tilde{S}|\tilde{S}_{ij}\tilde{S}_{ij}\rangle}, \quad (6)$$

where the brackets ($\langle\rangle$) represent an averaging operation. For the horizontal planes, this was an ensemble of the planar average at each downstream position. For the vertical planes, this was an ensemble of the average along the streamwise direction at each downstream position.

3. RESULTS

3.1 *SFS Statistics*

Scale-dependence of the SFS quantities is observed when the filter width is varied and the SFS transfer rate of kinetic energy is calculated. Means and standard deviations of Π^H_Δ (see Table 1) indicate that the SFS behavior changes when the filter scale becomes the same order of magnitude as the measurement height and fall within the production subrange of the kinetic energy spectrum ($z/\Delta \lesssim 1$). Furthermore, the behavior of Π^H_Δ depends on the streamwise position in the flow as the mean and standard deviations decrease with distance away from the roughness transition. This dependence is also observed in the probability density functions of Π^H_Δ, as shown in Fig. 9. The intermittency of the SFS transfer rate of kinetic energy (identified as elevated tails of the PDFs) decreases with distance downstream from the roughness transition.

Calculations of the SFS transfer rate of kinetic energy using the vertical fields, Π^V_Δ show similar trends though at much greater magnitude since the predominant vertical gradient of filtered velocity is included in the surrogate calculation. Fig. 10 shows mean profiles of Π^V_Δ at varying distances downstream of the roughness transition. The dramatic decrease in magnitude of Π^V_Δ downstream of the roughness transition indicates that the transition has a large impact locally on the SFS dynamics.

3.2 *A-priori Evaluation of Model Coefficients*

Values of the model coefficient, C_s, calculated from the PIV measurements using Eq. 6, range from 0.12 to 0.16. These values are in general agreement with past *a priori* studies. Mean profiles of C_s^2 are shown in Fig. 11 and indicate that C_s^2, at a given level near the surface, decreases as the distance from the roughness transition increases. This trend agrees with the conclusions of a recent LES study of the ABL over heterogeneous terrain using scale-dependent dynamic subgrid-scale models in conjunction with Lagrangian averaging to compute C_s^2 (Stoll and Porté-Agel, 2006). In that study, C_s^2 was found to adjust to the decreasing mean shear and flow anisotropy over the rough-to-smooth surface transition by increasing near the transition but then gradually decreas-

Table 1: Dependence of SFS transfer rate of kinetic energy on filter scale (units of m^2/s^3).

Filter Scale:	$\frac{x}{\Delta}$	$\frac{z}{\Delta} = 0.36$	$\frac{z}{\Delta} = 0.72$	$\frac{z}{\Delta} = 1.44$
$\Pi^H_\Delta\|_A$ ($\sigma_{\Pi^H_\Delta}$)	0.5	3.9(17.0)	3.6(12.8)	3.1(9.1)
$\Pi^H_\Delta\|_B$ ($\sigma_{\Pi^H_\Delta}$)	1.5	2.4 (8.6)	2.3(6.3)	2.0(4.4)
$\Pi^H_\Delta\|_C$ ($\sigma_{\Pi^H_\Delta}$)	2.5	1.8(6.7)	1.7(4.9)	1.5(3.5)
$\Pi^H_\Delta\|_S$ ($\sigma_{\Pi^H_\Delta}$)	–	1.3(5.0)	1.1(3.7)	0.9(2.6)

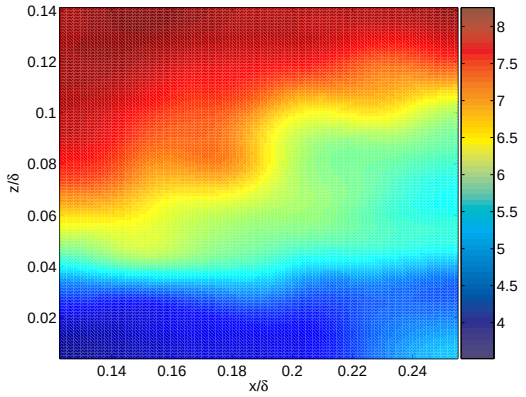

FIG. 7: Vertical field of filtered streamwise velocity field ($\tilde{u}_1, m/s$) from PIV measurements at x/δ = 0.5 behind a rough-to-smooth surface transition.

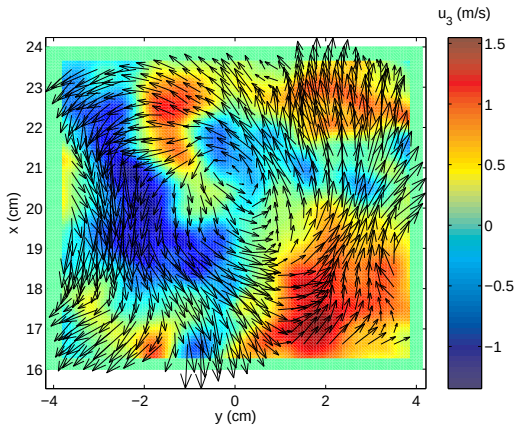

FIG. 8: Horizontal field of filtered vertical velocity overlaid with filtered velocity fluctuation vectors from stereoscopic PIV measurements at x/δ = 0.5 and z/δ = 0.05 behind a rough-to-smooth surface transition.

ing back to equilibrium levels found over a homogeneous surface.

To evaluate the performance of SFS modeling in LES, an *a priori* test of the SFS eddy-viscosity model is performed using the model coefficients calculated from Eq. 6 with the horizontal PIV data. The results, as expected, demonstrate the inability of the eddy-viscosity model to accurately model local SFS dynamics, proven by the low correlation between the measured and modeled SFS cross-stress, $\rho(\tau_{13}^{meas}, \tau_{13}^{ev}) \sim 0.3$. A single horizontal plane of τ_{13}^{meas}, shown in Fig. 12, obviously has different local features than that of τ_{13}^{ev} calculated based on the same filtered velocity field. This agrees with previous *a priori* studies of eddy-viscosity type models (e.g., Liu *et al.*, 1994).

4. CONCLUSIONS

Results of this novel wind tunnel study on the effects a of roughness transition on SFS modeling in LES have shown that the change in surface roughness has a large impact on the SFS stresses and transfer rate of kinetic energy. The results show that there is a dependence of the SFS transfer rate of kinetic energy on the location in the flow. The magnitude and standard deviation of the SFS transfer rate of kinetic energy as well as its intermittent behavior decreases with downstream distance away from the transition. The results also show that the eddy-viscosity model coefficient decreases with downstream distance from the transition. This agrees with the results of recent LES studies using Lagrangian scale-dependent dynamic SFS models. The inability of the eddy-viscosity model to accurately predict local features of the flow has been demonstrated by performing an *a priori* test of the model and resulted in a low correlation between the measured and modeled SFS stress, agreeing with previous studies. Finally, the unique data set and framework presented here provide motivation for a more thorough and

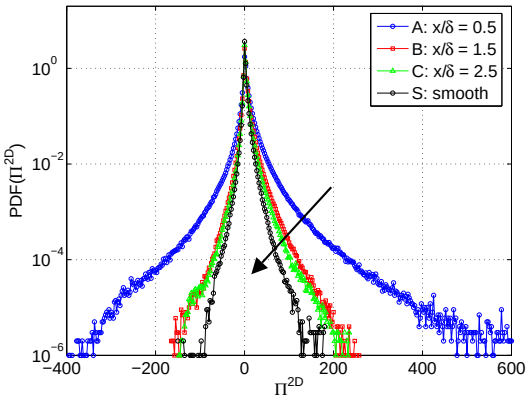

FIG. 9: Probability distribution functions (PDFs) of SFS transfer rate of kinetic energy for various positions in the flow. The arrow follows the PDFs from the furthest upstream position ("A") to the downstream limit of a smooth surface ("S").

complete study of the effects of filter scale and model formulation to better understand how LES can be improved to become a more reliable tool to study the atmospheric boundary layer over heterogeneous surface conditions.

5. ACKNOWLEDGMENTS

This work was supported by NSF (grants EAR-0537856 and EAR-0120914 as part of the National Center for Earth-surface Dynamics) and NASA (grant NNG06GE256). Computer time was provided in part by the Minnesota Supercomputing Institute. MAC was supported by a University of Minnesota Doctoral Dissertation Fellowship.

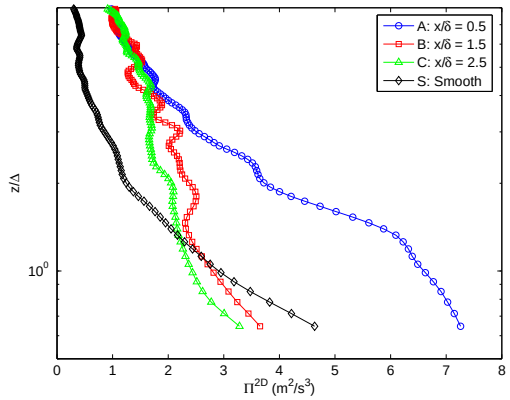

FIG. 10: Mean profiles of the SFS transfer rate of kinetic energy, Π_Δ^V (Eq. 3), downstream of a rough-to-smooth surface transition, evaluated *a priori* using high-resolution PIV measurements.

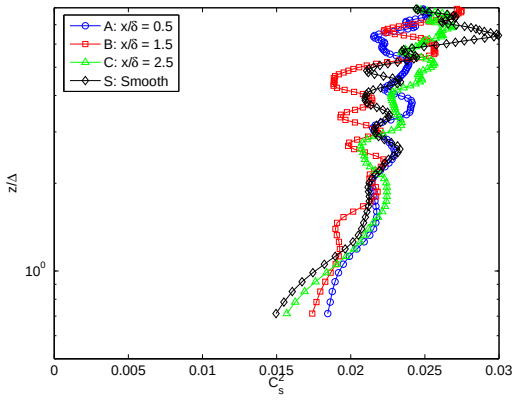

FIG. 11: Mean profiles of the Smagorinsky coefficient, C_s^2 (Eq. 6), downstream of a rough-to-smooth surface transition, evaluated *a priori* using high-resolution PIV measurements.

REFERENCES

Antonia, R. A. and Luxton, R. E., 1971: The response of a turbulent boundary layer to a step change in surface roughness. Part 1. Smooth-to-rough *J. Fluid Mech.*, **48**(4), 721-761.

Antonia, R. A. and Luxton, R. E., 1972: The response of a turbulent boundary layer to a step change in surface roughness. Part 2. Rough-to-smooth *J. Fluid Mech.*, **53**(4), 737-757.

Bou-Zeid, E., Meneveau, C. and Parlange, M. B., 2004: LES of neutral atmospheric boundary layer flow over heterogeneous surfaces: blending height and effective surface roughness. *Water Resources Res.* **40**.

Bou-Zeid, E., Meneveau, C., and Parlange, M. B., 2005: A scale-dependent Lagrangian dynamic model for large-eddy simulation of complex turbulent flows. *Phys. Fluids*, **17**.

Bradley, E. F., 1968: A micrometeorological study of velocity profiles and surface drag in the region modified by a change in surface roughness. *Quart. J. of Roy. Meteorol. Soc.*, **94**, 361-379.

Carper, M. A., Porté-Agel, F., 2004: The role of coherent structures on subfilter-scale dissipation rates of turbulence measured in the atmospheric surface layer, *J. Turbulence*, **5** 040.

Cheng, H. and Castro, I. P., 2002: Near-wall flow development after a step change in surface roughness. *Bound. Layer Meteor*, **105**, 411-432.

Elliot, W. P., 1958: The growth of the atmospheric boundary layer. *Trans. Amer. Geophys. Union*, **39**, 1048-1054.

Higgins, C. W., Parlange, M. B. and Meneveau, C., 2003: Alignment trends of velocity gradients and subgrid-scale fluxes in the turbulent atmospheric boundary layer. *Bound. Layer Meteor.*, **109**, 59-83.

Horst, T. W., Kleissl, J., Lenschow, D. H., Meneveau, C., Moeng, C.-H., Parlange, M. B., Sullivan, P. P. and Weil, J. C., 2004: HATS: Field observations to obtain spatially filtered turbulence fields from crosswind arrays of sonic anemometers in the atmospheric surface layer. *J. Atmos. Sci.*, **61**, 1566-1581.

Jiménez, J., 2004, Turbulent flow over rough walls. *Annu. Rev. Fluid Mech.*, **36**, 173-196.

Kaimal, J. C. and Finnigan, J. J., 1994: *Atmospheric Boundary Layer Flows*, 289 pp., Oxford University Press.

Kleissl, J., Meneveau, C. and Parlange, M. B., 2004: Field experimental study of dynamic Smagorinsky models in the atmospheric surface layer. *J. Atmos Sciences* **61**, 2296-2307.

Liu S., Meneveau C. and Katz J., 1994: On the properties of similarity subgrid-scale models as deduced from measurements in a turbulent jet. *J. Fluid Mech.*, **275**, 83-119.

Meneveau, C. and Katz, J., 2000 Scale-invariance and turbulence models for large-eddy simulation. *Annu. Rev. Fluid Mech.*, **32**, 1-32.

Mulhearn, P. J., 1978: A wind-tunnel boundary-layer study of the effects of a surface roughness change: rough to smooth. *Bound. Layer Meteor.*, **15**, 3-30.

Porté-Agel, F., Meneveau, C. and Parlange, M. B., 2000: A scale-dependent dynamic model for large-eddy simulation: application to a neutral atmospheric boundary layer. *J. Fluid Mech.*, **415**, 261-284.

Porté-Agel, F., Parlange, M. B., Meneveau, C. and Eichinger, W. E., 2001: A-priori field study of the subgrid-scale heat fluxes and dissipation in the atmospheric surface layer. *J. Atmos. Sci.*, **58**, 2673-2698.

Porté-Agel, F., 2004: A scale-dependent dynamic model for scalar transport in large-eddy simulations of the atmospheric boundary layer. *Bound. Layer Meteor.*, **112**, 81-105.

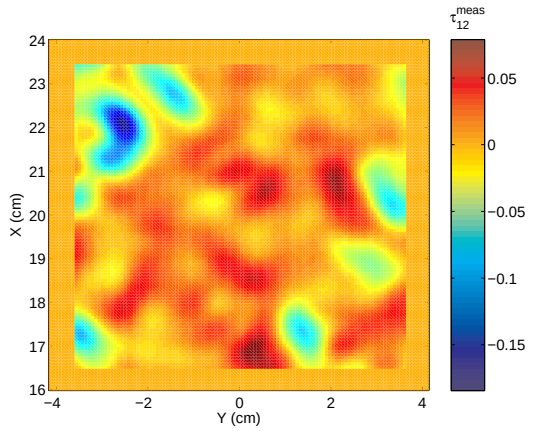

FIG. 12: Contours of SFS stress, τ_{ij} (Eq. 1), calculated based on a horizontal field of filtered velocity.

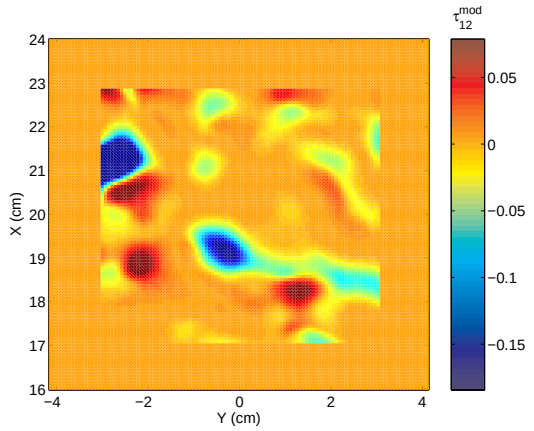

FIG. 13: Contours of the modeled SFS stress using a eddy-viscosity model, τ_{ij}^{ev} (Eq. 2) based on the same horizontal field of filtered velocity used to calculate the actual SFS stress shown in Fig. 12.

Stoll, R. and Porté-Agel, F., 2006: Dynamic subgrid-scale models for momentum and scalar fluxes in large-eddy simulation of neutrally stratified atmospheric boundary layers over heterogeneous terrain. *Water Resources Res.*, 2006.

Stoll, R. and Porté-Agel, F., 2006: Surface heterogeneity effects on regional-scale fluxes in stable boundary layers: an LES study. *AMS 17th BLT Symposium, San Diego, CA*, **JP4.2**.

Sullivan, P.P, Horst, T. W., Lenschow, D. H., Moeng, C.-H. and Weil, J. C., 2003: Structure of subfilter-scale fluxes in the atmospheric surface layer with application to large-eddy simulation modeling. *J. Fluid Mech.*, **482**, 101-139.

Tong, C., Wyngaard J. C., Khanna S. and Brasseur, J. G., 1998: Resolvable- and subgrid-scale measurement in the atmospheric surface layer: technique and issues, *J. Atmos. Sci.*, **55** 3114-3126.

Wood, D. H., 1982: Internal boundary layer growth following a step change in surface roughness, *Bound. Layer Meteor.*, **22**, 241-244.

Westerweel, J., 1997: Fundamentals of digital particle image velocimetry. *Meas. Sci. Technol.*, **8**, 1379-1392.